JMEPEG (2022) 31:3471–3480
https://doi.org/10.1007/s11665-021-06464-y

1059-9495/$19.00

TECHNICAL ARTICLE

Experimental Investigation on Influence of Waste Egg Shell Particles on Polylactic Acid Matrix for Additive Manufacturing Application

G.S. Sivagnanamani, S. Rashia Begum, R. Siva, and M. Saravana Kumar

Submitted: 11 October 2020 / Revised: 23 October 2021 / Accepted: 13 November 2021 / Published online: 1 December 2021

Biodegradable polymer plays a major role in Additive Manufacturing (AM) technologies due to its novel characteristics that include its complete degradability and eco-friendly nature. The present research work aims to obtain smooth and stable Poly Lactic Acid (PLA)/Eggshell particles (E) composite filaments with enhanced mechanical and thermal properties for additive manufacturing applications. Composite filaments were developed by varying the ratio of E/PLA to 4-6-8-10-12 weight percentages (wt.%) using a single screw extruder. A study of physical, chemical, mechanical, and thermal properties for the manufactured filaments was made. The extruded filaments were subjected to thermal analysis using Melt Flow Index (MFI) to obtain the optimum value for AM applications. XRD analysis made on 4 wt.% eggshell revealed a higher crystallinity than neat PLA. The thermal results of neat PLA and various weight compositions of E revealed there is a decrease in thermal stability and thermal decomposition due to an increase in filler content. 4 wt.% of E shows the good tensile strength of 49.29 MPa with smooth and stable E/PLA composite filaments during extrusion. The SEM images of the composites revealed the interaction between the filler and the matrix. Based on the experimental work, it is observed that the addition of eggshell powder into the PLA increases the mechanical properties with an optimum content of 4 wt.% of E.

Keywords additive manufacturing, composite filaments, eggshell particles, FDM, material extrusion, polymer composite

1. Introduction

Over the past few decades, the development and modification of biodegradable polymers have helped the eradication of sustainable issues based on petrochemical-based polymers (Ref 1, 2). For the past few years, biodegradable polymers have been obtained from renewable resources, such as poly (butylene adipate-co-terephthalate), starch, polyhydroxy butyrate, poly (lactic acid), and polycaprolactone. Poly (lactic acid) (PLA) is a conventional polymer and is the first commodity plastic produced from annually renewable resources (Ref 3-5). PLA which is biodegradable, recyclable, and thermoplastic in nature was obtained from renewable resources such as sugar cane, potatoes, and other biomasses (Ref 5, 6). PLA granules have been used considering their organic degradable nature and their major role in the 3D printing and medical scaffolding application. The main beneficial application of the PLA material lies in the biomedical applications that include bone scaffolds. PLA materials have some drawbacks that include sensitivity to water, limited impact, fast aging, and inherent brittleness. These were rectified by the addition of the filler materials.

PLA matrix requires blending with the low-cost renewable fillers for making eco-friendly materials with superior properties. One of the important renewable fillers (Chicken eggshell) has been used in this research work. Chicken eggshell, used as the filler material because of its easy availability and low price (Ref 7), is the by-product obtained from the poultry industry in which it is considered as one of the worst environmental crises, mostly in the well-developed egg production industry. Eggshell has 95% of calcium carbonate in the form of calcite and the remaining 5% has organic materials such as type X collagen, sulfated polysaccharides, and other proteins (Ref 8). Hence, eggshell particles were used as the filler materials for superior properties. Availability and its chemical properties indicate it as a potential source of filler in polymer composite films.

Boparai et al., developed Nylon6 Al_2O_3 based composite filament for FDM using a single screw extruder to match the property of commercial ABS and evaluated it for rheological thermal and mechanical properties. The results showed composite material having high wear resistance and thermal stability (Ref 9). Antonia et al., fabricated PLA magnesium composite filaments and manufactured ACL screws for medical implant applications and characterized it using FTIR, SEM, and DSC. The results showed implant can maintain structural integrity (Ref 10). Daver et al., blended cork with PLA to manufacture biodegradable filament for 3DPrinting applications and made a comparison with compressed molded samples

G.S. Sivagnanamani and **S. Rashia Begum**, Department of Mechanical Engineering, College of Engineering, Anna University, Chennai, Tamil Nadu, India; **R. Siva**, Department of Mechanical Engineering, Sathyabama Institute of Science and Technology, Chennai, Tamil Nadu, India; and **M. Saravana Kumar**, Department of Production Engineering, National Institute of Technology, Tiruchirappalli, Tamil Nadu, India. Contact e-mail: mxesiva@gmail.com.

and characterized for thermal-mechanical and rheological properties. The outcome showed the addition of cork filers reducing tensile strength and increasing the impact strength of PLA (Ref 11). Singh et al., reinforced Al_2O_3 powder to nylon6 polymer for the development of filament for FDM applications. SEM image showed an even distribution of the particles. MFI results were matched with neat ABS to obtain the correct percentage of particles and carried out a statistical analysis on wear results which showed the composites having high wear rate (Ref 12). Esposito et al., have proposed a novel composite biomaterial with PLA and Lecce Stone (LS) scrap. Researchers have recommended the use of LS as a filler particle which has high impact values on the environment (Ref 13). Wu et al., printed synthetic trabecular bone models with PLA and HAP composites by FDM. Researchers have done scanning of the trabecular bone using Computer tomography imaging technique and developed it into a 3d model. The developed model was tested for compression and screw pull-out tests. Materials were characterized using FTIR and SEM results showed mechanical properties as closer to natural bone and a decrease in the accuracy of FDM parts with the addition of HAP (Ref 14). Heidari et al., manufactured continuous carbon fiber reinforced PLA parts by modifying the extruder setup and compared it with pure PLA. Morphological analysis showed the bonding between fiber and PLA matrix. A three-point bending test and tensile tests were carried out and the results showed a significant improvement in composites compared to PLA (Ref 15). Boparai et al., optimized process parameters of a single screw extruder for nylon-Al2O3 composites and developed alternative filament for 3D printing applications. Taguchi method was used in the interruption of the significance of various input parameters. ANOVA table showed material composition and die temperature having a greater impact on the stiffness of the filament (Ref 16). Singh et al., developed a multi-material specimen through FDM and tests for mechanical and thermal stability. Recycled ABS, PLA, and HIPS were used in the development of three-layered specimens. The results showed improvement in the tensile strength of HIPS to 28.81 kg/mm^2. The authors concluded that multi-materials have the feasibility to print 3D parts and play a major role in developing smart materials and structures through 4D printing (Ref 17, 18). Abdullah et al., compared Polyamide PA12 with PA12 ceramic composites and checked for mechanical and biological characteristics. Zirconia and beta-tricalcium phosphate were mixed with polyamide at different ratios for the extrusion of the filament. The outcome showed an increase in the tensile modulus and impact strength of the composites by 8-31 and 98-181%, respectively. Researchers also suggest the material as suitable for FDM for use as particular craniofacial implants for low-income patients (Ref 19). Donate et al., studied mechanical, biological, and morphological characters of Calcium carbonate, beta-tricalcium phosphate with PLA composites through variations in the percentage of ceramics. Results showed an increase in porosity and surface roughness which led to good metabolic activity, composition with PLA: caco3: β-TCP-95:2.5:2.5 showed better results and thus need for further evaluation for the BTE process (Ref 20). Janek et al., extruded composite filament with 50-50% Hap-Polyvinyl alcohol and compared it with commercial PLA composite. Tensile strength of prepared filament was seen as three times lower than commercial PLA-Gypsite filament (Ref 21). Weng et al., observed mechanical and thermal properties of ABS/montmorillonite (OMMT) composites prepared through the use of the melt intercalation method. The outcome showed an increase in the tensile strength of the composite by 43% while the increase in injection molded samples was by 28.9%. Thermal stability and shrinkage ratio also increased with the addition of the OMMT composite. The authors suggest the material as suitable for 3DPrinting applications (Ref 22). Boparai et al., studied the thermal properties of waste nylon 6 - Al/Al_2O_3 composites to check the feasibility of material for FDM applications. Uniform distribution of particles was achieved which showed improvement in the thermal stability and crystallinity of the polymer with the addition of fillers (Ref 23). Rahimizadeh et al., recycled fiberglass turbine blades and converted them into reinforcement to polymer filaments for FDM applications. The prepared filaments were checked for mechanical properties outcome and comparison with neat PLA showed improvement in the ultimate strength and elastic modulus by 10 and 16% and increase in young's modulus by 8% and without any significant improvement seen in the tensile strength (Ref 24). Literature review reveals limited work carried out in the development of composite filaments with specific properties. Despite most of the research work carried out with metal, natural fibers, synthetic fibers, and ceramics with PLA, ABS, PETG, PCL none has been done with natural ceramics.

The focus of this work is on the development of composite filaments using waste materials (eggshell particles), with different composition range for additive manufacturing applications.

2. Materials and Methods

2.1 Materials

Multipurpose extrusion grade PLA with a specific gravity of 1.24g/cc and a peak melting temperature of 160 °C has been used in this research work. The PLA material (Ingeo Biopolymer 4043D) purchased from the NATURE Tec India Pvt limited was in the form of granules Fig. 1(a). Eggshells collected from local restaurants were rinsed in distilled water several times and were furnace heat-treated for 3 hours at 110 °C for removal of the soft inner layer of the eggshell. The eggshells were crushed using a high-energy ball milling machine Fig. 1(b) and sieved through 500 BSS mesh for obtaining particles of size less than 25microns Fig. 1(c).

2.2 Extrusion of Filament

PLA granules and Eggshell particles were dried in a hot air oven for the elimination of the residual moisture. The fine ESP particles uniformly dispersed in toluene were allowed for coating on the granules. A custom-made filament extruder Fig. 1(d) was incorporated for the manufacture of ESP - PLA composite filaments of diameter 1.75mm Fig. 2(b). by varying the ESP weight fraction as 4, 6, 8, 10, and 12%. In addition, to achieve the homogeneous distribution of ESP in PLA, the filament extrusion process was repeated three times (Ref 25-27) using the single screw extruder as shown in Fig. 2(c).

2.3 X-ray Diffraction Analysis

X-Ray Diffractometer (XRD) was used for the determination of the phase structure of PLA-ESP composites using CuKα

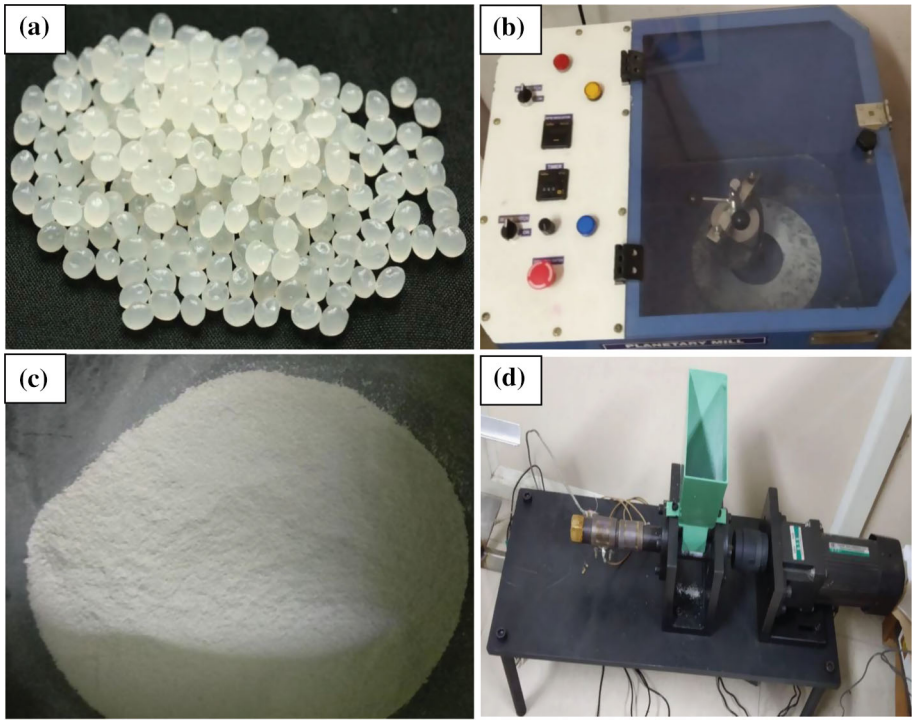

Fig. 1 (a) PLA granules (b) Ball mill (c) Eggshell particles after processing (d) Single Screw extruder

radiation (λ = 1.54178 Å) at 20 k and 10 mA. The diffraction angle, 2theta was measured between 0° to 80° with a step size of 0.05 and scanning rate of 2°/min using Enraf (Bruker) nonius CAD4 single-crystal X-ray diffractometer

2.4 Fourier Transform Infrared Spectroscopy

Perkin Elmer system one: FTIR spectrometer with scanning range of 4000-500 cm-1 at 1.0 cm -1 resolution was used to study the presence of functional groups in PLA/ESP polymer composites

2.5 Melt Flow Index

Melt Flow Index of the various PLA-ESP composite filaments was performed using a Global calibration device in accordance with ASTM D1238 standard.

2.6 TGA/DSC Analysis

PLA composite filaments with various weight percentages of eggshell particles (4, 6, 8, 10, and 12%) were analyzed for thermogravimetric and Calorimetric Analysis using NETZSCH STA 449 F3 Jupiter equipment. PLA-ESP composite filament sample of an average weight of 10mg is heated between 28 and 600 °C at a heating rate of 10 °C/min under nitrogen environment (10mL/min). The same thermal cycle was used for obtaining the calorimetric data during the TGA analysis.

2.7 Scanning Electron Microscope

Hitachi-S3400N scanning electron microscope combined with EDS facility was used for the study of the distribution of ESP in the filament, surface, and the cross-sectional morphology of the composite filament. A study of the Microstructure of the surfaces was made using SEM images with a magnification ranging from 30× to 5000×.

2.8 Mechanical Testing

Tinius Olsen Universal testing machine with 50 kN capacity was used for carrying out the tensile test for PLA/E composites Fig. 3(a) and (b). Figure 2(a) shows tensile test specimens prepared as per ASTM D638 standard. A set of five samples were tested for ensuring the reliability of the data and the average has been considered for evaluation.

3. Results and Discussion

3.1 XRD Analysis

The XRD pattern of eggshell powder, neat PLA, and E/PLA composite are shown in Fig. 4 (a), (b) and (c). The peaks in eggshell Fig. 4(a) are well fitted revealed the major composition of $CaCO_3$ presence with higher crystallite. The presence of $CaCO_3$ supports the hardness presence of the eggshell. The peak of $CaCO_3$ that appeared at 2θ = 29.5° resulting (104) plane, indicates the rhombohedral structure (Ref 28). The calculated crystallinity index of the eggshell was 76.06%. Figure 4(b) shows the neat PLA XRD pattern. Two broad peaks were observed at 2θ = 16.92° and 19.28° indicating (110) and (203) planes along with the sharp peaks 2θ = 37°, 44.04°, 64.24°, and 77.3° confirmed the amorphous structure of neat PLA. The high crystalline peak plane (110) confirmed the presence of α-form crystals in PLA. The calculated crystallinity index of neat PLA was 41.19%. Figure 4(c) shows the E/PLA composite XRD pattern. It was noted that the PLA intensity become weaker with no clear peaks in the E/PLA composite due to the incorporation of crystallite eggshell powder. In addition, the peak of eggshell powder at 2θ = 29.5° incorporated at peak 2θ = 29.28° of E/PLA composite confirmed the crystallinity eggshell interaction. These two observations

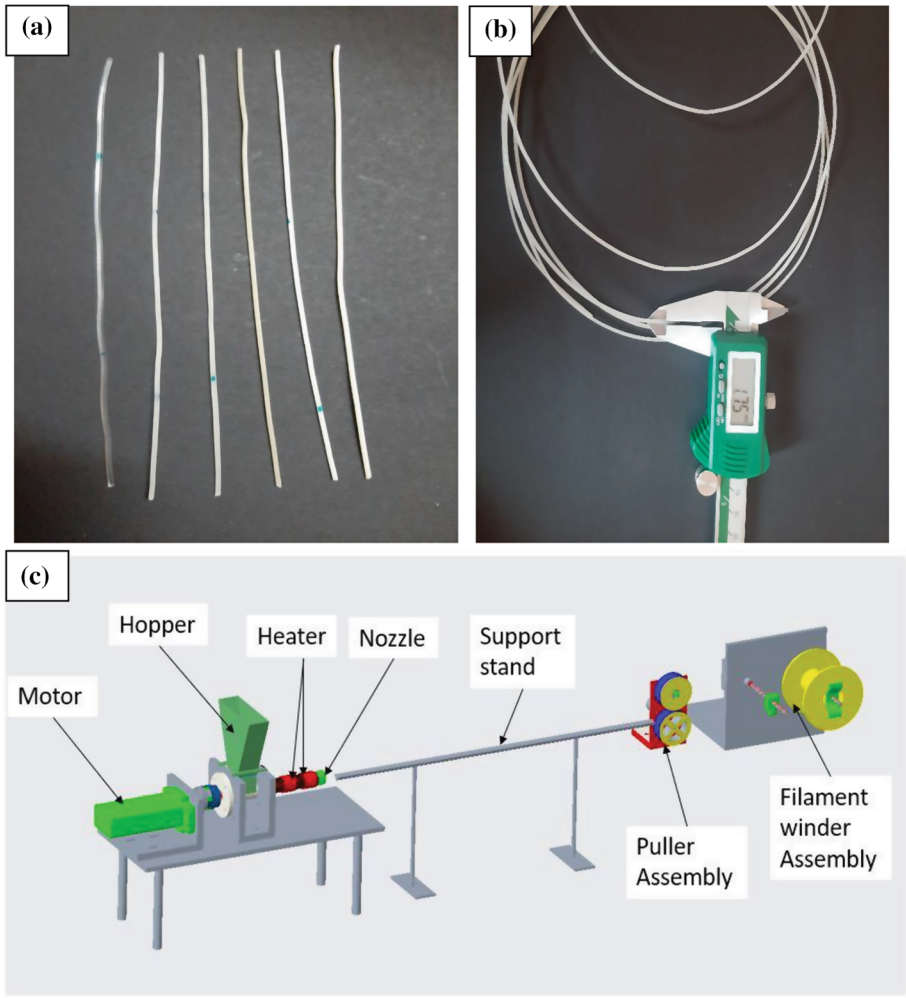

Fig. 2 (a) Tensile test specimen (b) Filament with 1.75mm diameter (c) Schematic diagram of single screw extruder

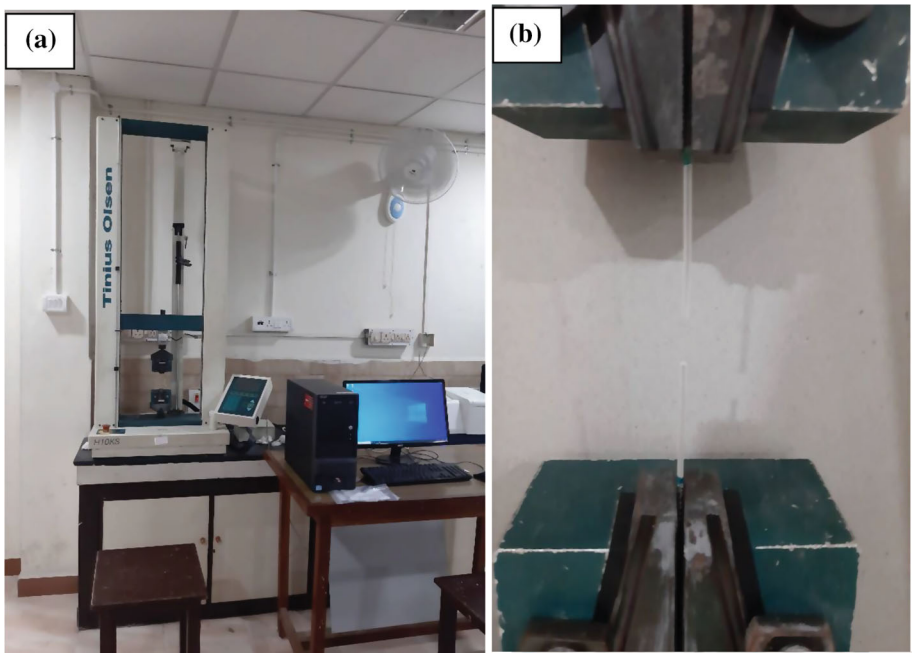

Fig. 3 (a) Tinius Olsen Universal testing machine (b) Filament holder with tensile specimen

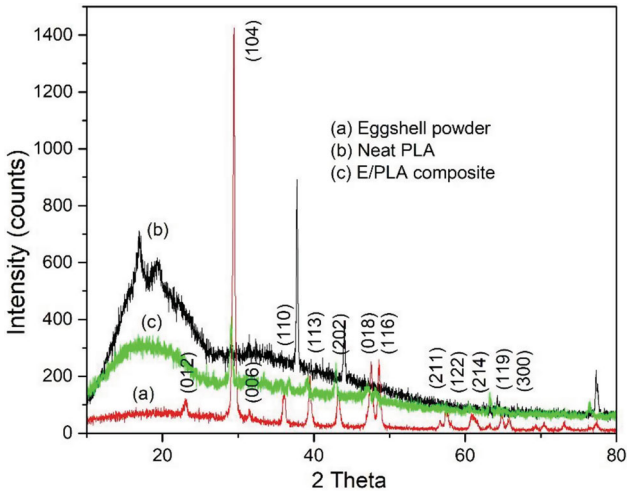

Fig. 4 XRD analysis of PLA and its composite filaments (a) Eggshell powder (b) Neat PLA (c) E/PLA composites

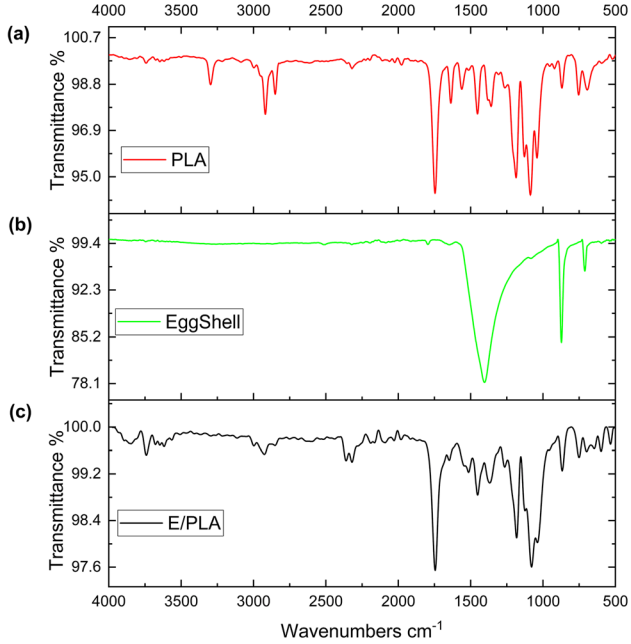

Fig. 5 FTIR spectra of PLA filaments and its composites (a) PLA (b) eggshell particles (c) E/PLA

confirmed the PLA and Eggshell interaction in the composite by affected crystallinity E/PLA composite (Ref 29). The calculated crystallinity index of E/PLA was 55%. This increased crystallinity index result confirmed the presence of highly crystalline eggshells in the PLA in the E/PLA composite. It confirms the eggshell powder accelerates the crystallization of PLA by acting as a nucleating agent (Ref 30).

3.2 FTIR Characterization

FTIR for Neat PLA, Eggshell powder, and 12%E/PLA composites were measured, the peak and frequency are shown in Fig. 5(a)–(c). The frequency and peak in Fig. 5(a) correspond to the neat PLA. PLA was formed with a rich carbon chain corresponding to C=O groups. The sharp peaks at 693.99 and 753.42 cm^{-1}, besides high transmittance sharp peaks at 1746.07 cm^{-1} were assigned for C=O group stretching vibration (carbonyl of ester group), which confirms the presence of rich carbon (Ref 31). The peaks 1041.92, 1088.76, 1128.51, 1185.98, and 1263.57 cm^{-1} as corresponding to the C-O groups. The peak 953.83 and 869.3 cm^{-1} corresponds to a C-C group single bond. The peaks 1452.96 and 2997.62 cm^{-1} correspond to the asymmetric stretching vibration of C-H groups stretching in the CH_3 and C-H groups Symmetric stretching of CH_3 (Ref 32). The peak 1358.7 cm^{-1} corresponds to C-H groups CH-Bending. The peak 3296.70 cm^{-1} corresponds to –OH group bending and stretching vibration. $–CH_3$ symmetric vibration in the side chains was observed at peak 2850.27 cm^{-1} (Ref 30, 33). The frequency and peak in Fig. 5(b) correspond to the eggshell powder. The intense sharp peak at 1404.38 cm^{-1} corresponds to carbonate groups of stretching, confirming the presence of carbonate. The peak at 710.72 and 872.83 cm^{-1} correspond to the calcium carbonate ($CaCO_3$) existence with the in-plane and out-plane deformation. The peak at 3647.55 and 2513.13 cm^{-1} corresponds to the presence of hydroxyl group stretching where weak intensity indicates the sample containing less water molecule. The peaks 1795.31 and 1646.36 cm^{-1} correspond to C=O group carbonyl stretching (Ref 34), the frequency and peak in Fig. 5(c) correspond to E/PLA composite. It is observed that the peaks associated with the E/PLA were mostly correlated with the PLA sample, and no new peaks were observed, indicating the predominant physical interaction of PLA and eggshell powder. However, the peak at 3296.70 cm^{-1} was seen corresponding to –OH group bending and the stretching vibration of PLA got disappeared in the E/PLA composite. The peak at 693.99 cm^{-1} of PLA corresponds to C=O group stretching vibration nearly disappeared. The peak at 1746.07 cm^{-1} increased intensity observed for the E/PLA composite. The peak at 1636.77 cm^{-1} of PLA was shifted to a higher peak at 1647.93 cm^{-1} of E/PLA composite corresponding to C=O group carbonyl stretching of eggshell powder. At peak 1264.85 and 1038.78 cm^{-1} increased intensity was observed due to hydrogen bonds (Ref 29).

3.3 Melt Flow Index Value

Initially, the MFI value of the PLA was 9.4 g/10min. Analysis of the MFI readings was made by varying the percentage of the eggshell filaments such as 4, 6, 8, 10, and 12% at 155 °C constant temperature with 2.16kg constant load Fig. 6. PLA with 4% of ESP showed 11.2 g/10min, PLA with 6% of ESP showed 13.2 g/10min, PLA with 8% of ESP showed 15.4 g/10min, PLA with 10% of ESP showed 17.7 g/10min and PLA with 12% of ESP showed 22.5 g/10min. The results indicated an increase in the MFI value with an increase in the percentage of the eggshell filler materials due to the density difference with respect to higher viscosity. The melting point of the PLA was in the range of 130-180 °C, but the melting point of the ESP was high, hence at the temperature of 155 °C PLA melts but the eggshell particles pressurize the PLA due to higher density which leads to more melting of PLA. So, the MFI value increases with the increase in the egg shell particles as shown in Fig. 6. So, it was evident that the 4% of the egg sell particles must be suitable for the 3D printing application because of its low melt flow index of 11.2 g/10 min.

3.4 TGA Analysis

The TGA curves of neat PLA, 4, 6, 8, 10, and 12% E/PLA composites were compared and details are shown in Fig. 7. It is essential to find a suitable processing temperature based on applications to avoid degradation of composites (Ref 34). The TGA curves of all composites followed a similar pattern with a single-stage decomposition. The degradation of composites started at temperatures 294.09, 283.03, 282.05, 277.17, 255.21, and 244.96 °C for neat PLA, 4, 6, 8, 10, and 12% E/PLA composites with a minor weight loss from the room temperature. Generally, considerable weight loss occurs for raw eggshell till 400 °C due to their water absorption (hydrophilic nature). However major weight loss differences had not been observed between neat PLA and E/PLA composites indicate the polymers which covered the eggshell might protect the degradation process of the eggshell (Ref 35). It is noted that the addition of eggshell percentage attained a decrease in the thermal stability with a maximum temperature of 49 °C for 12% E/PLA composite than neat PLA composite, confirming the different pathways of the neat PLA. The presence of Ca in the eggshell resulted in a decrease in the thermal stability in the eggshell percentage composites (Ref 36). A significant weight loss was noted at the degradation stage. The degradation of composites ended at temperature 370.5, 365.17, 356.88, 355.90, 350.53, and 349.56 °C for Neat PLA, 4, 6, 8, 10, and 12% E/PLA with a minimum total weight loss of 79.7% for 12% E/PLA and maximum total weight loss of 97.13% for the neat PLA. Which had no further weight loss due to its complete degradation. Whereas, the eggshell initial degradation exhibited at 400 °C with a minimum weight loss due to the decomposition of components like chitin, protein, and polysaccharides was observed from Fig. 7 on eggshell percentage composites (Ref 37). Generally, in eggshell particles major degradation occurs between 700 and 850 °C due to $CaCO_3$ gets converted into CaO. The eggshell percentage composite caused a reduction in the percentages noted as higher than the neat PLA composites due to the eggshell particle presence which is not decomposed in the temperature analyzed.

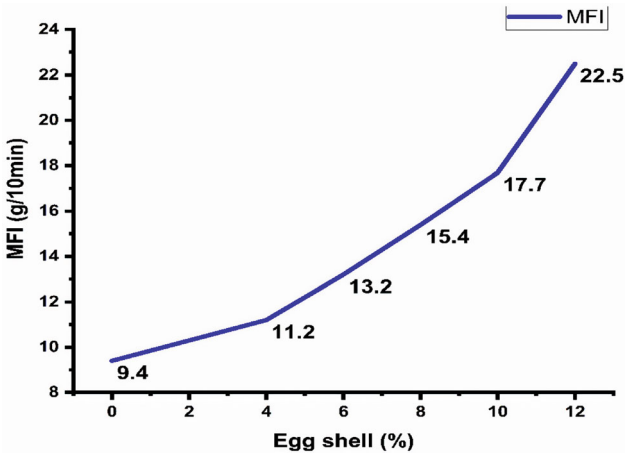

Fig. 6 Melt flow index (g/10min) Vs ESP (%)

3.5 DSC Analysis

DSC curves of neat PLA, 4, 6, 8, 10, and 12% E/PLA composites were made and details are shown in Fig. 8. The degradation, melting, cold crystallization, glass transition of PLA composites were visible, confirming it as semi-crystalline polymers from sharp glass transition temperature endothermic peak 67.28 °C. The glass transition temperatures of 4, 6, 8, 10, and 12% E/PLA composites were found to be 78.07 °C exhibiting a temperature higher than neat PLA composite with exothermic peaks due to the evolution of carbon dioxide from calcium carbonate from the eggshell (Ref 38). The increased temperature was due to the movement of PLA chains hindered by the addition of eggshell particles (Ref 39). The cold crystalline for neat PLA was seen lying at 107.19 °C as an exothermic peak and for 4, 6, 8, 10, and 12% E/PLA composites was seen lying at 109.95, 111.79, 112.72, 114.02, and 114.02 °C as an exothermic peak. The temperature increase resulted in an increase in molecular mass and eggshell presence. The mobility of the polymer chain with greater

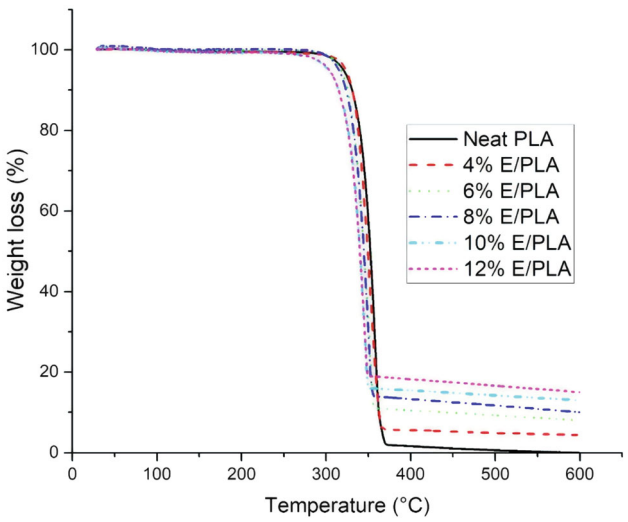

Fig. 7 TGA analysis of various compositions of eggshell particles compared to pure PLA

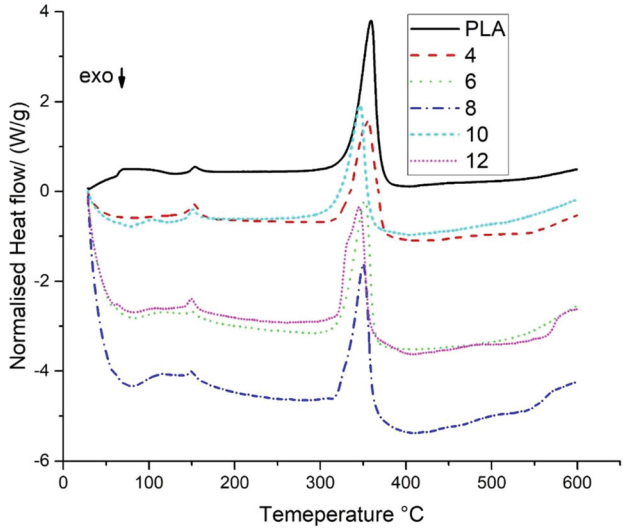

Fig. 8 DSC analysis of various compositions of eggshell particles compared to pure PLA

flexibility of PLA crystallization occurred earlier under the same heating condition (Ref 36). It was observed that the melting point of the neat PLA occurs at 154.20 °C and for 4, 6, 8, 10, and 12% E/PLA composites lies at 152.74, 149.67, 149.54, 148.67, and 148.67 °C as endothermic peaks. The observation showed a decrease in the melting temperature due to the addition of the eggshell percentages on the composite. Due to restriction on the crystalline material development by eggshell particles acted as an obstacle. The sharp endothermic peaks at 358.79 °C for neat PLA and 355.6, 351.87, 350.1, 346.06, and 345.49 °C for 4, 6, 8, 10, and 12% E/PLA composites were observed, showing the degradation temperature of PLA in the composites.

3.6 Surface Morphology

The SEM images of the E/PLA composite are shown in Fig. 9(a)–(d). The longitudinal section of the E/PLA composite Fig. 9(a) and (b) shows a smooth surface with a wavy pattern due to the material property variations and possible attributed impurities presence. The presence of wavy pattern like a ridged structure could be due to the movement of the extrusion head and affected by the retention of heat in the filament. The cross-sectional view of the E/PLA composite is shown in Fig. 9(c) and (d). The clean-cut image represents the brittleness of the filament due to the addition of a high percentage of eggshell particles. Coagulation of the eggshell particle in some places was seen. In many places, it was distributed well as like platelet formation (Ref 40). Less coagulation resulted in the uniform distribution of the eggshell particle achieved even at higher percentage addition with the PLA. A strong interfacial adhesion was present due to the porous fibril structure surface of the eggshell particle, which was responsible for the good adsorbing capacity to react with the PLA (Ref 41). The PLA was well surrounded over the eggshell particle with smaller gaps indicating a better interfacial adhesion between the PLA and eggshell particle (Ref 42). In addition, the hydrophilic behavior of eggshell and PLA resulted in better interfacial adhesion between the PLA. From Fig. 9(c) the E/PLA filament is seen with less pull-out eggshell particle confirming a better interfacial adhesion between eggshell and PLA.

3.7 Tensile Strength

Tensile strength of neat PLA and E/PLA composites were examined to study the effect of ESP weight percentage on the mechanical properties. Figure 10 shows the composite filament before and after testing of composite filaments. Tensile test results of neat PLA, 4% E/PLA, 6% E/PLA, 8% E/PLA, 10% E/PLA and 12% E/PLA stress-strain curve was shown in Fig. 11. The tensile strength of 4% E/PLA (49.29 MPa) exhibited higher tensile strength than the neat PLA due to the attraction of reinforced filler eggshell with the matrix. Further addition of eggshell fillers resulted in a decrease in tensile strength which may be due to the agglomeration of eggshell into the matrix. Crack formation leads to the fiber pull-out due to the increase in eggshell filler percentages resulting in lesser tensile strength. In addition, an increase in tensile modulus for the E/PLA composites supports the tensile strength decrease due to the incorporation of eggshell filler. Lower and higher tensile modulus were observed on 4% E/PLA (1.89 GPa) and 12% (2.39 GPa). The elongation at break for the neat PLA, 4% E/PLA, 6% E/PLA, 8% E/PLA, 10% E/PLA, and 12% E/PLA was observed decreases by the addition of eggshell filler content. This could be due to eggshell filler restriction on the chain movement of PLA its stiffening action. The elongation at break was seen strongly affected by a lack of interaction between the filler and the matrix, increased volume content of the filler, and improper dispersion of the filler and the matrix. The higher and lower elongation at break was observed on 4% E/PLA (6.614%) and 12% (1.72% GPa). The agglomeration, dispersion, crack and pull-out of eggshell filler with the matrix are shown clearly in the SEM analysis to support tensile strength analysis (Table 1).

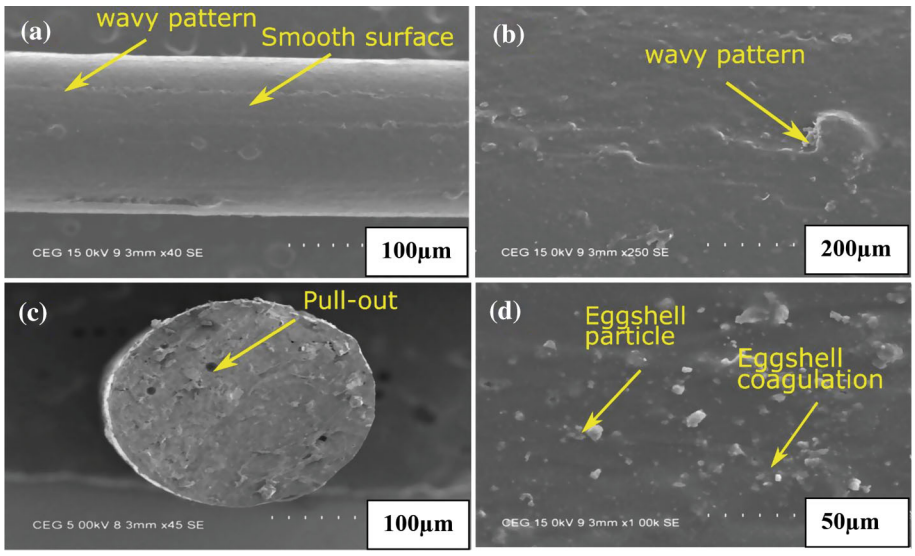

Fig. 9 SEM images of E/PLA composite (a) and (b) Surface of the filament (c) fractured section (d) Surface showing the presence of eggshell particles

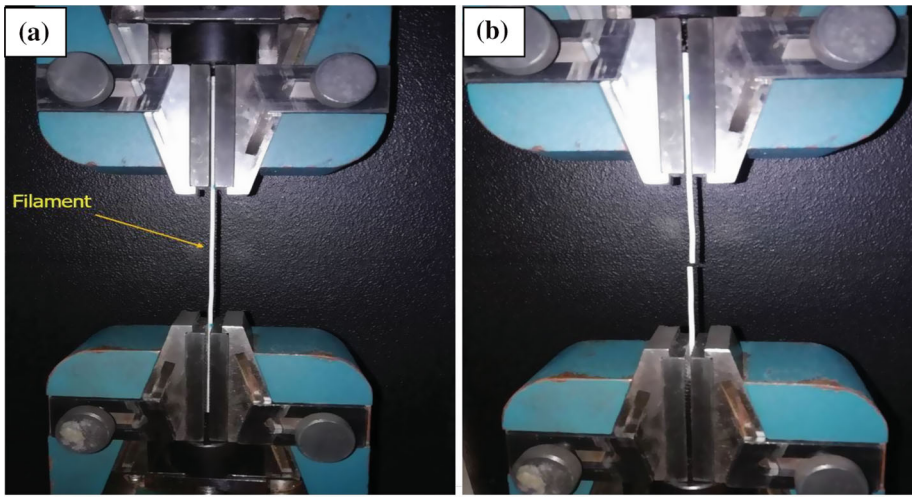

Fig. 10 Composite filaments (a) Before tensile test (b) After tensile test

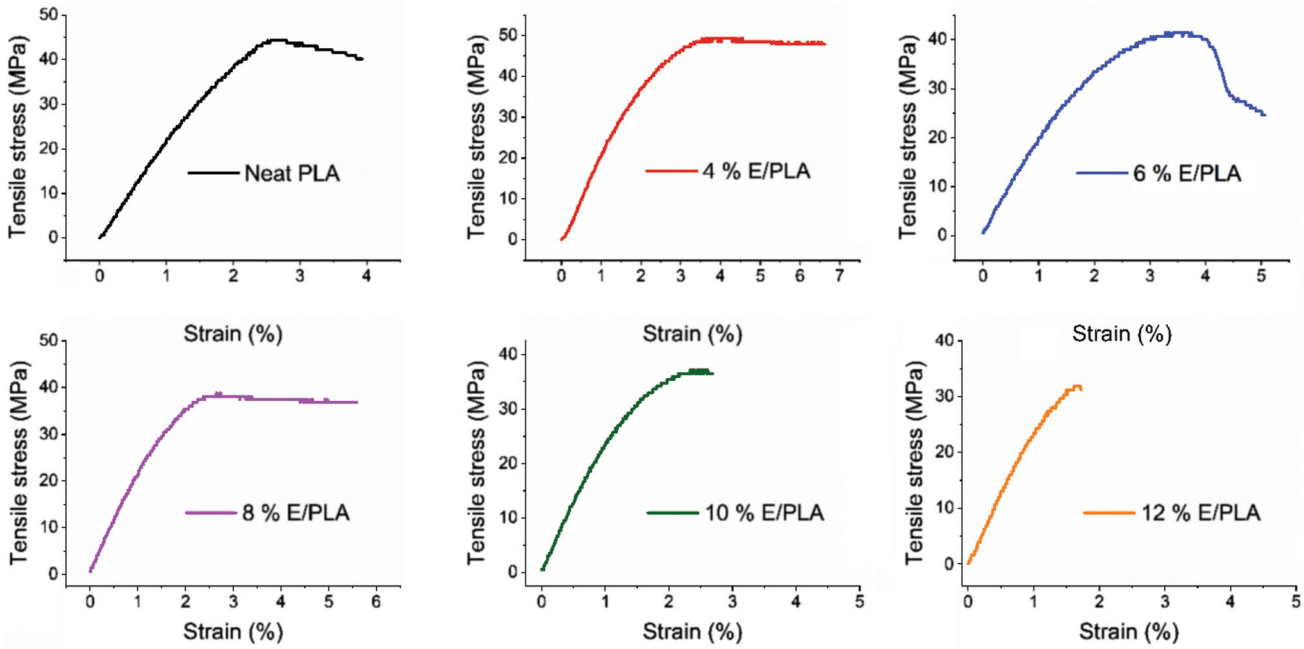

Fig. 11 Stress-Strain curve for E/PLA composites

Table 1 Single Screw extruder specifications

L/D ratio	Heating zone, °C	Screw speed, rpm	Nozzle diameter, mm	Filament diameter, mm
10.25	170	15	1.61	1.75

4. Conclusion

The results of the thermal, mechanical, and morphological analysis lead to the following conclusions;

- The XRD analysis made on 4% eggshell revealed a higher crystallinity than neat PLA. the PLA intensity (counts) became weaker with no clear peaks in the E/PLA composite due to the incorporation of crystallite eggshell powder.
- The TGA results on neat PLA and various eggshell particles revealed there is a decrease in thermal stability and thermal decomposition due to an increase in the filler content. The eggshell percentage composite residues percentages were seen as higher than the neat PLA composites due to the eggshell particle presence which is not decomposed in the temperature analyzed.
- MFI values for 4% of ESP was 11.2 g/10min which was

the optimum value for 3D printing applications and an increase in the melt flow Index value was seen with the increase in the percentage of the eggshell filler materials this was due to the fact that the density difference with respect to higher viscosity.

- 4% of the ESP shows good tensile strength of 49.29 MPa with smooth and stable PLA/eggshell composite filaments during extrusion and it was evident that the presence of more amount of eggshell fillers decreases the mechanical properties of the composite filament.
- Uniform distribution of the ESP was obtained in 4% of the filler materials compared to the 8, 10, and 12% of the eggshell fillers. This was due to the possibility of clustering in the higher concentration of the eggshell fillers, the crack formation and the breakage of filaments occurs which affects the mechanical properties.
- Despite the inferiority of mechanical properties of the composite to the commercial neat PLA, the added ESP caused an increase in the thermal properties with respect to composition and can be used for 3D printing applications.

Acknowledgment

The authors thank the Centre for Research, Anna University, Chennai-600025. For the financial support in the form of fellowship (Anna Centenary Research Fellowship, ACRF) (Ref. No. CFR/ACRF/2018/AR1/5).

References

1. X. Tian, T. Liu, Q. Wang, A. Dilmurat, D. Li and G. Ziegmann, Recycling and Remanufacturing of 3D Printed Continuous Carbon Fiber Reinforced PLA Composites, *J. Clean. Prod.*, 2017, **142**, p 1609–1618
2. R. Siva, G. Gopinatha, I. MouliPremchand, G. Mathiselvan, M. SaravanaKumar. Study on Morphological and Mechanical Properties on Treated and Untreated Veldt Grape/PLA Composites. Materials Today Proceedings, https://doi.org/10.1016/j.matpr.2021.06.425
3. M.A. Kreiger, M.L. Mulder, A.G. Glover and J.M. Pearce, Life Cycle Analysis of Distributed Recycling of Post-consumer High Density Polyethylene for 3-D Printing Filament, *J. Clean. Prod.*, 2014, **70**, p 90–96
4. S.R. Begum, M.S. Kumar, C.I. Pruncu, M. Vasumathi and P. Harikrishnan, Optimization and Fabrication of Customized Scaffold Using Additive Manufacturing to Match the Property of Human Bone, *J. Mater. Eng. Perform.*, 2021 https://doi.org/10.1007/s11665-020-05449-7
5. Z. Liu, Q. Lei and S. Xing, Mechanical Characteristics of Wood, Ceramic, Metal and Carbon Fiber-Based PLA Composites Fabricated by FDM, *J. Market. Res.*, 2019, **8**(5), p 3741–3751
6. Sivagnanamani, G. S., Ramesh, P., Kumar, M. H., and Arul Mozhi Selvan, V. (2021). Fracture Analysis of Fused Deposition Modelling of Bio-composite Filaments. In *Fracture Failure Analysis of Fiber Reinforced Polymer Matrix Composites* (pp. 71-84). Springer, Singapore
7. S. Kumar and A. Czekanski, Development of Filaments Using Selective Laser Sintering Waste Powder, *J. Clean. Prod.*, 2017, **165**, p 1188–1196
8. V. Hembrick-Holloman, T. Samuel, Z. Mohammed, S. Jeelani and V.K. Rangari, Ecofriendly Production of Bioactive Tissue Engineering Scaffolds Derived from Egg-and Sea-Shells, *J. Market. Res.*, 2020, **9**(6), p 13729–13739
9. Boparai, K. S., Singh, R., & Singh, H. (2016). Experimental Investigations for Development of Nylon6-Al-Al2O3 Alternative FDM Filament. *Rapid Prototyp. J*
10. I. Antoniac, D. Popescu, A. Zapciu, A. Antoniac, F. Miculescu and H. Moldovan, Magnesium Filled Polylactic Acid (PLA) Material for Filament Based 3D Printing, *Materials*, 2019, **12**(5), p 719
11. F. Daver, K.P.M. Lee, M. Brandt and R. Shanks, Cork–PLA Composite Filaments for Fused Deposition Modelling, *Compos. Sci. Technol.*, 2018, **168**, p 230–237
12. R. Singh, S. Singh and F. Fraternali, Development of In-house Composite Wire Based Feed Stock Filaments of Fused Deposition Modelling for Wear-Resistant Materials and Structures, *Compos. B Eng.*, 2016, **98**, p 244–249
13. C.E. Corcione, E. Palumbo, A. Masciullo, F. Montagna and M.C. Torricelli, Fused Deposition Modeling (FDM): An Innovative Technique Aimed at Reusing Lecce Stone Waste for Industrial Design and Building Applications, *Constr. Build. Mater.*, 2018, **158**, p 276–284
14. Wu, D., Spanou, A., Diez-Escudero, A., & Persson, C. (2020). 3D-Printed PLA/HA Composite Structures as Synthetic Trabecular Bone: A Feasibility Study Using Fused Deposition Modeling. *J. Mech. Behav. Biomed. Mater.*, *103*, 103608
15. Heidari-Rarani, M., Rafiee-Afarani, M., & Zahedi, A. M. (2019). Mechanical Characterization of FDM 3D Printing of Continuous Carbon Fiber Reinforced PLA Composites. *Compos. Part B: Engineering*, *175*, 107147
16. Boparai, K. S., Singh, R., & Singh, H. (2016). Process Optimization of Single Screw Extruder for Development of Nylon 6-Al-Al2O3 Alternative FDM Filament. *Rapid Prototyp. J.*
17. R. Singh, R. Kumar, I. Farina, F. Colangelo, L. Feo and F. Fraternali, Multi-material Additive Manufacturing of Sustainable Innovative Materials and Structures, *Polymers*, 2019, **11**(1), p 62
18. K.S.S. Kumar, M. Vivekananthan, M. Saravanakumar and F.S. Raj, Investigation of Physico Chemical, Mechanical and Thermal Properties of the Guettarda Speciosa Bark Fibers, *Materials Today: Proceedings*, 2021, **37**, p 1845–1849. https://doi.org/10.1016/j.matpr.2020.07.443
19. A.M. Abdullah, T.N.A.T. Rahim, W.N.F.W. Hamad, D. Mohamad, H.M. Akil and Z.A. Rajion, Mechanical and Cytotoxicity Properties of Hybrid Ceramics Filled Polyamide 12 Filament Feedstock for Craniofacial Bone Reconstruction via Fused Deposition Modelling, *Dent. Mater.*, 2018, **34**(11), p e309–e316
20. R. Donate, M. Monzón, Z. Ortega, L. Wang, V. Ribeiro, D. Pestana and R.L. Reis, Comparison Between Calcium Carbonate and β-Tricalcium Phosphate as Additives of 3D Printed Scaffolds with Polylactic Acid Matrix, *J. Tissue Eng. Regen. Med.*, 2020, **14**(2), p 272–283
21. M. Janek, V. Žilinská, V. Kovár, Z. Hajdúchová, K. Tomanová, P. Peciar and Ľ. Bača, Mechanical Testing of Hydroxyapatite Filaments for Tissue Scaffolds Preparation by Fused Deposition of Ceramics, *J. Eur. Ceram. Soc.*, 2020, **40**(14), p 4932–4938
22. Z. Weng, J. Wang, T. Senthil and L. Wu, Mechanical and Thermal Properties of ABS/Montmorillonite Nanocomposites for Fused Deposition Modeling 3D Printing, *Mater. Des.*, 2016, **102**, p 276–283
23. K.S. Boparai, R. Singh, F. Fabbrocino and F. Fraternali, Thermal Characterization of Recycled Polymer for Additive Manufacturing Applications, *Compos. B Eng.*, 2016, **106**, p 42–47
24. Rahimizadeh, A., Kalman, J., Fayazbakhsh, K., & Lessard, L. (2019). Recycling of Fiberglass wind Turbine Blades into Reinforced Filaments for Use in Additive Manufacturing. *Compos. Part B: Eng.*, *175*, 107101
25. L. Delva, K. Ragaert, J. Degrieck and L. Cardon, The Effect of Multiple Extrusions on the Properties of Montmorillonite Filled Polypropylene, *Polymers*, 2014, **6**(12), p 2912–2927
26. D. Filgueira, S. Holmen, J.K. Melbø, D. Moldes, A.T. Echtermeyer and G. Chinga-Carrasco, Enzymatic-Assisted Modification of Thermomechanical Pulp Fibers to Improve the Interfacial Adhesion with Poly(lactic acid) for 3D Printing, *ACS Sustain. Chem. Eng.*, 2017, **5**(10), p 9338–9346
27. Wang, P., Zou, B., Ding, S., Huang, C., Shi, Z., Ma, Y., & Yao, P. (2020). Preparation of Short CF/GF Reinforced PEEK Composite Filaments and Their Comprehensive Properties Evaluation for FDM-3D Printing. *Compos. Part B: Eng.*, *198*, 108175
28. Z. Lule and J. Kim, Nonisothermal Crystallization of Surface-Treated Alumina and Aluminum Nitride-Filled Polylactic Acid Hybrid Composites, *Polymers*, 2019, **11**(6), p 1077

29. B. Ashok, S. Naresh, K.O. Reddy, K. Madhukar, J. Cai, L. Zhang and A.V. Rajulu, Tensile and Thermal Properties of Poly(lactic acid)/Eggshell Powder Composite Films, *Int. J. Polym. Anal. Charact.*, 2014, **19**(3), p 245–255
30. R. Nasrin, S. Biswas, T.U. Rashid, S. Afrin, R.A. Jahan, P. Haque and M.M. Rahman, Preparation of Chitin-PLA Laminated Composite for Implantable Application, *Bioactive Mater.*, 2017, **2**(4), p 199–207
31. Yuniarto, K., Purwanto, Y. A., Purwanto, S., Welt, B. A., Purwadaria, H. K., & Sunarti, T. C. (2016, April). Infrared and Raman Studies on Polylactide Acid and Polyethylene Glycol-400 Blend. In *AIP Conference Proceedings* (Vol. 1725, No. 1, p. 020101). AIP Publishing LLC
32. Brito, G. F., Agrawal, P., & Mélo, T. J. (2016, September). Mechanical and Morphological Properties of PLA/BioPE Blend Compatibilized with E-GMA and EMA-GMA Copolymers. In *Macromolecular Symposia* (Vol. 367, No. 1, pp. 176-182)
33. Huang, Y. Z., Ji, Y. R., Kang, Z. W., Li, F., Ge, S. F., Yang, D. P., Fan, X. Q. (2020). Integrating Eggshell-Derived CaCO3/MgO Nanocomposites and Chitosan into a Biomimetic Scaffold for Bone Regeneration. *Chem. Eng. J.*, *395*, 125098
34. M.S. Tizo, L.A.V. Blanco, A.C.Q. Cagas, B.R.B.D. Cruz, J.C. Encoy, J.V. Gunting and V.I.F. Mabayo, Efficiency of Calcium Carbonate from Eggshells as an Adsorbent for Cadmium Removal in Aqueous Solution, *Sustain. Environ. Res.*, 2018, **28**(6), p 326–332
35. J.P. Mofokeng, A.S. Luyt, T. Tábi and J. Kovács, Comparison of Injection Moulded, Natural Fibre-Reinforced Composites with PP and PLA as Matrices, *J. Thermoplast. Compos. Mater.*, 2012, **25**(8), p 927–948
36. E.H. Backes, L.D.N. Pires, L.C. Costa, F.R. Passador and L.A. Pessan, Analysis of the Degradation During Melt Processing of PLA/Biosilicate® Composites, *J. Compos. Sci.*, 2019, **3**(2), p 52
37. K. Kaewtatip, C. Chiarathanakrit and S.A. Riyajan, The Effects of Egg Shell and Shrimp Shell on the Properties of Baked Starch Foam, *Powder Technol.*, 2018, **335**, p 354–359
38. S.T. Morbale, S.S. Shinde, S.D. Jadhav, M.B. Deshmukh and S.S. Patil, Modified Eggshell Catalyzed, One-pot Synthesis and Antimicrobial Evaluation of 1, 4-dihydropyridines and Polyhydroquinolines, *Lett*, 2015, **7**, p 169–182
39. C.E. Tanase and I. Spiridon, PLA/chitosan/keratin Composites for Biomedical Applications, *Mater. Sci. Eng., C*, 2014, **40**, p 242–247
40. A. Potnuru and Y. Tadesse, Investigation of Polylactide and Carbon Nanocomposite Filament for 3D Printing, *Prog. Addit. Manuf.*, 2019, **4**(1), p 23–41
41. H. Daraei, A. Mittal, J. Mittal and H. Kamali, Optimization of Cr (VI) Removal onto Biosorbent Eggshell Membrane: Experimental & Theoretical Approaches, *Desalin. Water Treat.*, 2014, **52**(7–9), p 1307–1315
42. Y. Li, C. Han, Y. Yu, L. Xiao and Y. Shao, Crystallization Behaviors of Poly(lactic acid) Composites Fabricated Using Functionalized Eggshell Powder and Poly(ethylene glycol), *Thermochim. Acta*, 2018, **663**, p 67–76